SAGE-Hindawi Access to Research
International Journal of Electrochemistry
Volume 2011, Article ID 240837, 13 pages
doi:10.4061/2011/240837

Research Article

Effect of Elemental Composition on the Structure, Electrochemical Properties, and Ozone Production Activity of Ti/SnO_2-Sb-Ni Electrodes Prepared by Thermal Pyrolysis Method

Hamed Shekarchizade and Mohammad K. Amini

Chemistry Department, University of Isfahan, Isfahan 81744-73441, Iran

Correspondence should be addressed to Mohammad K. Amini, mkamini@chem.ui.ac.ir

Received 2 June 2011; Revised 26 August 2011; Accepted 17 September 2011

Academic Editor: Adalgisa Rodrigues de Andrade

Ti/SnO_2-Sb-Ni electrodes with various Ni- and Sb-doping levels have been prepared by dip-coating thermal pyrolysis procedure, and their simultaneous electrochemical ozone production (EOP) and oxygen evolution reaction (OER) were investigated. The effects of electrode composition on the nanostructure, morphology, electrochemical behavior, kinetic parameters, and lifetime of the electrodes were systematically studied using X-ray diffraction, scanning electron microscopy, cyclic voltammetry, linear sweep voltammetry, and chronopotentiometry. Dissolved ozone was produced in a quartz cell and its concentration was monitored by in situ UV spectrophotometry. The presence of small amounts of Ni (Ni : Sn atomic ratio of 0.2 : 100) gives valuable characteristics to the electrodes such as increasing EOP activity and service life. Higher Ni concentrations increase the electrode film resistance and decrease its capacitance, roughness factor, and service life, while increasing Sb level up to 12 atom% improves the electrode performance with respect to these parameters. Nevertheless, the Sb/Sn atomic ratio of more than 2% reduces the EOP current efficiency in favor of OER. The optimum composition of the electrode for EOP was determined to be Sb/Sn and Ni/Sn atomic ratios of 2% and 0.2%, respectively. The highest current efficiency was 48.3% in 0.1 M H_2SO_4 solution at room temperature.

1. Introduction

Ozone (O_3), as an environmentally friendly reagent with high oxidizing power, has found a broad range of applications in various fields such as water and wastewater treatment, sterilization of surgical equipments, bleaching processes, cleaning of semiconductor materials, and chemical synthesis [1–5].

There are two main methods for preparation of dissolved ozone: corona discharge followed by dissolving ozone into solution and electrolysis [6]. The latter method has the advantages of being a simple process which produces relatively high concentrations of ozone directly into solution without producing harmful nitrogen oxides and without need for a high voltage power source as compared to corona discharge.

The OER (1) is thermodynamically more favorable and severely competes with EOP (2) on the anode of an electrochemical ozone generator.

$$2\,H_2O \longrightarrow O_2 + 4\,H^+ + 4\,e^- \quad E^\circ = 1.23\,V \qquad (1)$$

$$3\,H_2O \longrightarrow O_3 + 6\,H^+ + 6\,e^- \quad E^\circ = 1.51\,V \qquad (2)$$

Consequently, minimizing OER is a key requirement for EOP with a reasonable current efficiency. This can be achieved by suitable choice of the anode material to have a high overpotential for OER. In addition, the anode should have good conductance, high durability under drastic operating conditions, and particularly good electrocatalytic activity for ozone production [1].

Beta lead dioxide (β-PbO_2) [7–11], Pt [12, 13], Pt composites [14, 15], boron-doped diamond [16–18], dimensionally stable anodes [19, 20], TiO_2 thin films on $Si/TiO_x/Pt$ substrate [21], and SnO_2-based catalysts [22, 23] are among the materials that have been used for EOP. Most of the investigations have been focused on β-PbO_2 which has shown a current efficiency of about 13% at room temperature [7]. Higher current efficiencies have been obtained in unusually concentrated acid solutions in the presence of fluoride or fluoride-containing species, applying very high current densities and cooling the anode-electrolyte interface to impractically low temperatures [7]. In addition, dissolution of poisonous Pb has limited the use of lead dioxide anodes. Recently, boron-doped diamond electrodes, due to their high conductivity, superior chemical, and dimensional stability as well as high overpotential for OER, have attracted much attention as novel anodes for EOP. A very high EOP current efficiency of 47% has been reported for a boron-doped diamond anode using a solid polymer electrolyte, the so-called "zero-gap" electrolytic cell [17].

SnO_2 is an n-type semiconductor with a band gap of 3.6 eV which crystallizes in a rutile-type structure. Although this oxide is quite inert toward chemical etching with common acids or alkalis, its electrical resistivity is very high at room temperature and thus cannot be directly used as electrode material. However, its conductivity can be significantly enhanced by addition of an appropriate dopant such as In(III), Sb(V), or F^- [24, 25]. Antimony-doped SnO_2 supported on titanium with high overpotential for OER has been widely used for the direct electrochemical conversion/combustion of organic pollutants in solution [26–29].

Wang et al. have reported Ni and Sb codoped SnO_2 on Ti foil as a promising electrode for EOP [23, 30]. They achieved a current efficiency of ~35% for ozone production in acidic solution at low applied voltage at room temperature. Later, this group investigated the effectiveness of the Ni and Sb codoped SnO_2 electrode for EOP in a membrane electrode assembly cell with convective flow system [31] and for electrochemical degradation of organic pollutants using 4-chlorophenol as a model toxic compound [32]. Recently, Christensen et al. [22] following the synthetic route reported by Wang et al. [30] reported EOP current efficiencies as high as 50% in 0.5 M sulfuric acid at a cell voltage of 2.7 V on electrodes containing Ni : Sn atomic ratio of 0.6 : 100 instead of 0.2 : 100 used by Wang et al. In spite of successful operation of Ti/SnO_2-Sb-Ni electrodes for ozone production, there is no information concerning the role of dopants on the electrochemical and morphological characteristics of these electrodes. The objective of the present work was to systematically investigate, for the first time, the effects of composition of the Ni and Sb codoped SnO_2 on the electrochemical behavior, kinetic parameters, morphology, nanostructure, and lifetime of the electrodes. Therefore, SnO_2 coatings with various Ni and Sb dopant levels were prepared by dip coating-thermal pyrolysis technique on titanium mesh substrates using the synthetic route reported by Wang et al. [30]. The correlation between electrode composition and its activity for simultaneous OER and EOP has been determined.

2. Experimental

2.1. Preparation of Titanium Mesh Anodes. The anodes were prepared using the synthetic route reported by Wang et al. [30], by dip coating from precursor solutions of $SnCl_4 \cdot 5H_2O$ (Aldrich), $SbCl_3$(Merck), and $NiCl_2 \cdot 6H_2O$ (Merck) dissolved in absolute ethanol (Merck), followed by thermal pyrolysis technique. To prepare anodes with different compositions, the $SnCl_4 \cdot 5H_2O$ concentration in ethanol solution was kept at 0.25 M, and the relative mole ratios of Sb/Sn and Ni/Sn were changed by varying the concentration of $SbCl_3$ and $NiCl_2 \cdot 6H_2O$ in the solution to obtain electrode coatings with varying concentrations of Sb and Ni in the ranges of 0–15 and 0-1 atom%, respectively, with respect to Sn. Therefore, all the reported Sb and Ni concentrations are in percent atomic ratios with respect to Sn in the coating solution.

An 8 × 8 mm titanium mesh, Dexmet Corporation, Pattern Designation 050 (LWD, 1.5 mm; SWD, 1 mm; strand width, 0.2 mm; opening per cm^2, ~130) spot-welded with 5 mm diameter titanium wires was used as the support. The mesh was etched in boiling 10% (w/v) aqueous oxalic acid solution for 1 h, rinsed with distilled water in an ultrasonic bath and dried. The etching process was performed to remove the well-adhered surface oxide layers and to provide a rough surface onto which the electrocatalyst can be more securely anchored. After pretreatment, the titanium substrates were dip-coated with the solution of precursors at room temperature, dried at 100°C for 10 min, and then heat treated at 500°C for another 10 min. This process was repeated 18 times until the desired oxide loading (2.5 mg cm^{-2}) was achieved. Finally, the electrodes were annealed at 500°C for 1 h, and the titanium wire surface was covered with an insulating rubber.

2.2. Physicochemical Characterization. The surface morphology of the electrodes was characterized using a Philips XL30 scanning electron microscope (SEM). X-ray diffraction (XRD) analysis of the samples was performed with a Bruker D8 Advance powder diffractometer using Ni filtered Cu K_α radiation (λ = 1.54056 Å) to characterize the structure of the electrodes. Since there was a high level of noise in the XRD pattern of the titanium mesh, these spectra were recorded on electrodes prepared from titanium foil (Aldrich, Cat. No. 36948-9) using the same coating method and conditions. All electrochemical measurements were performed with an Autolab potentiostat/galvanostat (Eco Chemie Model PGSTAT30) electrochemical system, controlled by the GPES software. The electrochemical cell was a homemade three-compartment glass apparatus (200 mL) with two porous separators (coarse glass frits) to avoid contact between the anodic (oxygen and ozone) and cathodic (hydrogen) gaseous products. Two platinum foils (1 × 4 cm) were employed as the counter electrodes at the opposite sides of the anode to ensure uniformity of the current on both faces. An Ag/AgCl, KCl (saturated) was used as the reference electrode in conjunction with a Luggin capillary to minimize the uncompensated ohmic drop. Before each measurement, the solution was purged with nitrogen gas. All measurements

were carried out at 25 ± 1°C. Stable voltammograms have been obtained after 3 scans between the cathodic and anodic limits. Polarization Tafel curves were recorded under quasistationary conditions (1 mV s^{-1}) in 0.1 M H_2SO_4 solution. Chronopotentiometric curves were recorded under anodic polarization conditions of 200 mA cm^{-2}.

2.3. Ozone Production and Measurement. In order to investigate the ozone production efficiency of the electrodes, the electrolysis was performed at a constant current density of 12 mA cm^{-2} in a standard spectrophotometer quartz cell containing 3 mL of 0.1 M H_2SO_4 solution at room temperature according to Wang et al. [30]. They have tested the accuracy of the in situ determination by UV spectroscopy, by indigo titration method. The ozone concentrations determined by the two methods were in agreement, indicating that the in situ UV determination was accurate and consistent. The working electrode was the modified titanium mesh anode placed flat at the bottom of the cell as shown in Figure 1. A platinum foil and an Ag/AgCl wire were used as the counter and reference electrodes, respectively. The concentration of dissolved ozone was measured in situ by a UV spectrophotometer (Cary-500, Varian,) at 258 nm using the molar absorption coefficient, ε, of 2900 L mol^{-1} cm^{-1} [31]. The current efficiency of the EOP process (Φ_{EOP}) was calculated according to Faraday's law from the following equation [13]:

$$\Phi_{EOP} = \left[\frac{nFCV}{It}\right], \quad (3)$$

where n is the moles of electrons transferred for one mole of ozone production which is equal to 6 according to (2), F is Faraday's constant, C is the concentration of produced ozone in the UV cell in mol L^{-1}, V is the volume of the electrolyzed solution in liter, I is the current used for electrolysis in A, and t is the electrolysis time in s. To have a consistent comparison, we calculated the current efficiency in the first 1 min of the constant current electrolysis experiment. Each calculated current efficiency was the average of 5 measurements.

3. Results and Discussion

3.1. Cyclic Voltammetry and Capacitance Measurements. Figure 2 shows cyclic voltammogram (CV) of a representative Ti/SnO_2-Sb-Ni electrode in 0.1 M H_2SO_4 solution. The voltammogram shows high capacitive currents in a wide potential range between 0.25 and 1.65 V without remarkable voltammetric features. At potentials more positive than 1.65 V, the anodic current rises due to the solvent oxidation (OER and EOP). All of the prepared electrodes showed high anodic overpotential for OER, which makes them highly suitable for the oxidation of organic compounds in aqueous solutions [26–29, 32]. The high cathodic current appeared at potentials less positive than 0.2 V, which is due to irreversible reduction of SnO_2 and hydrogen evolution reaction, which cause severe damage to the coated film, as reported previously [33, 34].

Capacitance measurements have been performed to determine the roughness factor (R_f) of different electrodes.

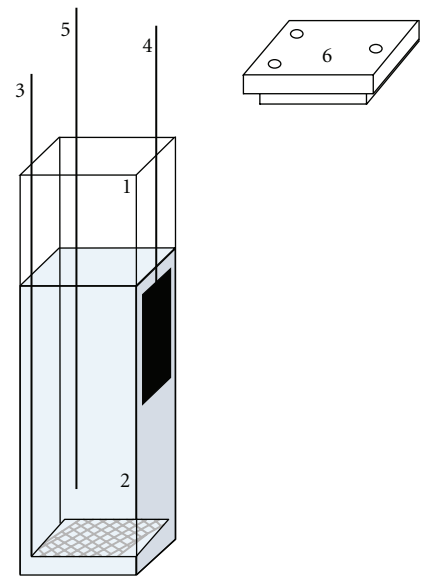

Figure 1: A schematic drawing of the electrolysis cell used for ozone production and in situ measurement showing (1) standard UV cells, (2) 0.1 M H_2SO_4 solution as the electrolyte, (3) modified Ti mesh anode, (4) Pt foil cathode, (5) Ag/AgCl wire reference electrode, and (6) cell cover.

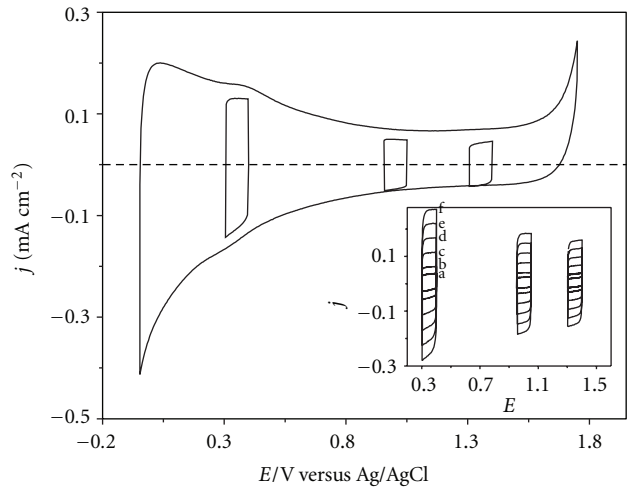

Figure 2: CVs of a representative Ti/SnO_2-Sb-Ni electrode between −0.05 and 1.75 V in three 100 mV ranges in 0.1 M H_2SO_4 solution. Scan rate: 50 mV s^{-1}. The inset shows CVs of the electrode in the three 100 mV ranges at different scan rates: 5, 10, 20, 30, 40, and 50 mV s^{-1} form a to f, respectively. The CVs at higher scan rates are not shown.

The CVs were recorded in three different 100 mV potential intervals at sweep rates of 5–1000 mV s^{-1}. Typical results are shown in the inset of Figure 2. The capacitance values were measured in the midpoints of the three potential ranges at 0.35, 1.0, and 1.35 V. The plots of the average current densities at the potential of 1.0 V, $(j_c + j_a)/2$, for the electrodes with different Ni and Sb dopant levels obtained at different scan rates are shown in Figures 3(a) and 3(b), respectively. Similar plots were obtained at 0.35 and 1.35 V (not shown). The linear relationship ($r > 0.999$) between

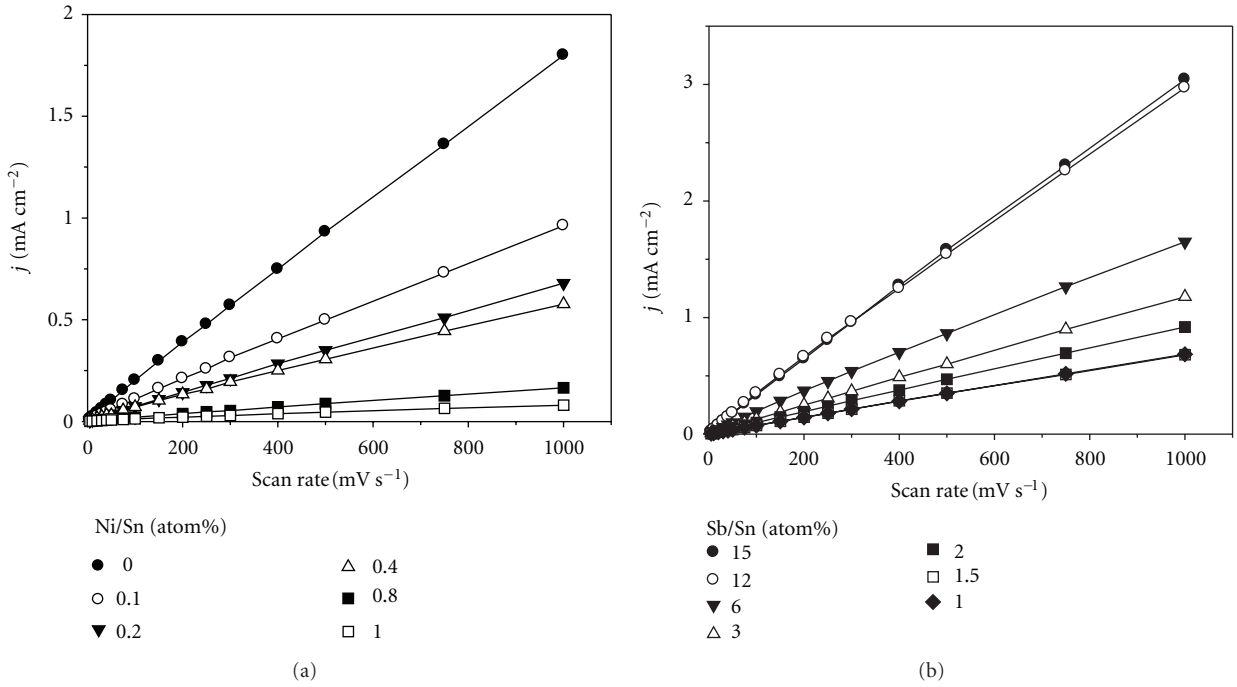

Figure 3: Variation of capacitive current density at 1.0 V with the potential scan rate measured between 0.95 and 1.05 V for (a) Ti/SnO_2-Sb(2%)-Ni(x%) and (b) Ti/SnO_2-Sb(x%)-Ni(0.2%) electrodes in 0.1 M H_2SO_4 solution. The values in parentheses are atomic ratios with respect to Sn.

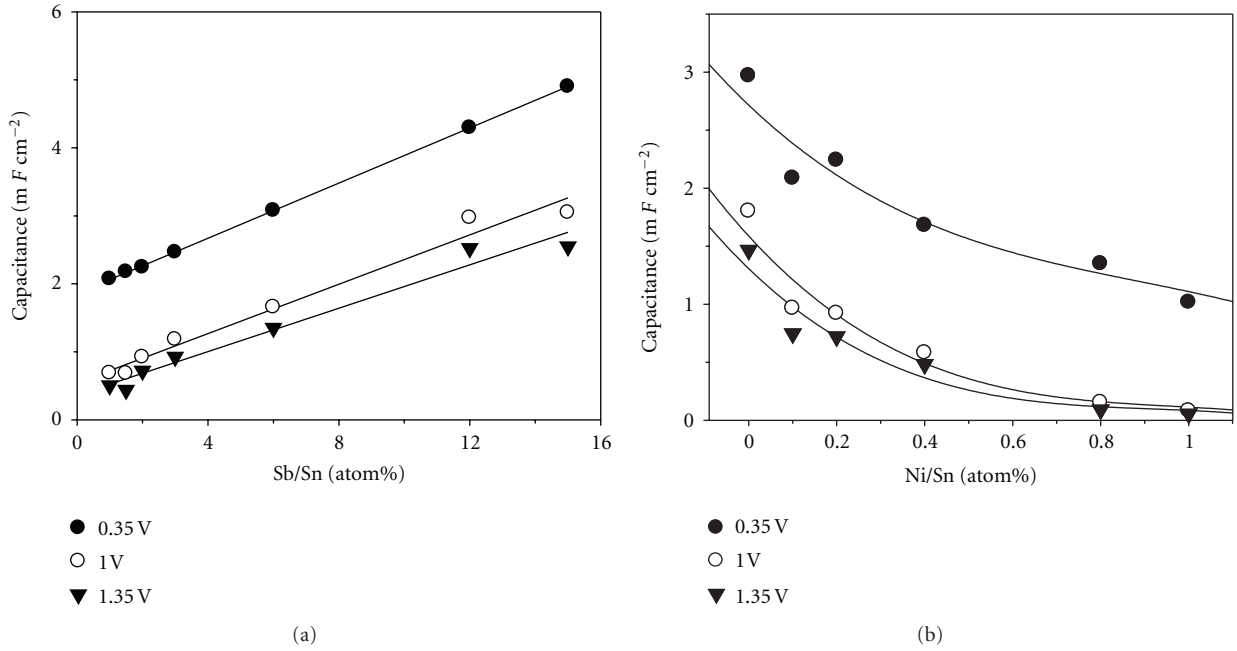

Figure 4: The effect of (a) Sb concentration in Ti/SnO_2-Sb(x%)-Ni(0.2%) and (b) Ni concentration in Ti/SnO_2-Sb(2%)-Ni(x%) electrodes on the values of capacitance at 0.35, 1.00, and 1.35 V. The values in the parentheses are atomic ratios with respect to Sn.

current density and scan rate for all of the electrodes confirms the nonfaradaic character of the current in these potential regions [34]. The capacitance at each potential was obtained from the absolute value of the slope of the corresponding straight line. Figures 4(a) and 4(b) show plots of the capacitance versus different concentrations of Sb and Ni, respectively. It can be seen, that the capacitance increases linearly with increasing the amount of Sb, Figure 4(a), while it decreases exponentially with increasing the concentration of Ni in the electrode, Figure 5(b). In addition, as shown in Figure 4, the capacitance is lower at higher potentials. This trend is in accordance with the Mott-Schottky relationship

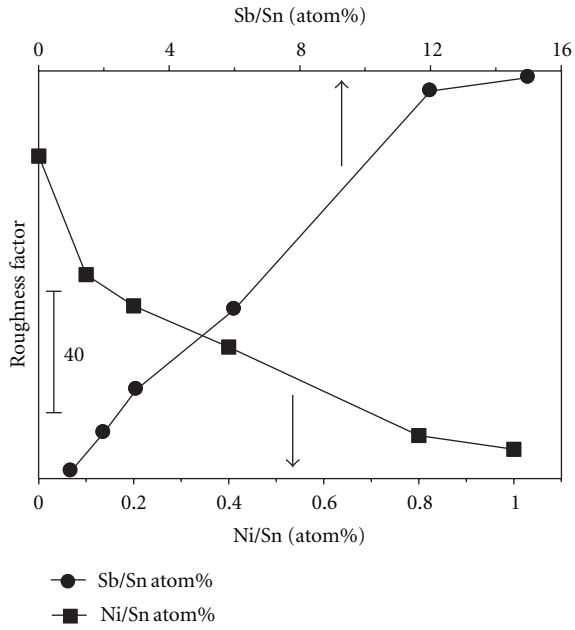

FIGURE 5: Variation of the estimated roughness factors (R_f) for Ti/SnO_2-Sb-Ni electrodes as a function of Sb and Ni concentrations. (•) Sb/Sn atom% and (■) Ni/Sn atom%.

for n-type semiconductors [34, 35]. The R_f-value, defined as real surface area per apparent geometric area, has been calculated according to a previously reported method [34, 36]. Figure 5 shows typical R_f-values at 1.0 V obtained for Ti/SnO_2-Sb-Ni electrodes prepared with different Sb and Ni contents. As can be seen, the R_f-value increases by increasing Sb content of the electrodes, suggesting an increase of the surface area exposed to the solution. However, Ni has a reverse effect, that is, the capacitance and R_f-values decrease by increasing the concentration of this element. The same behavior was observed for both elements at 0.35 and 1.35 V (not shown).

3.2. Ozone Generation. The electrolysis was carried out at a constant current of 12 mA cm^{-2} in 0.1 M H_2SO_4 solution on Ti/SnO_2-Sb-Ni electrodes prepared with different Sb and Ni concentrations (Sb/Sn and Ni/Sn atomic ratios of 0.0–15% and 0.0–1%, resp.). The concentration of ozone was measured as described in Section 2.3, and the current efficiency was calculated using (3). Figure 6(a) shows plot of the current efficiency for ozone production (Φ_{EOP}) as a function of Sb concentration at a fixed Ni/Sn atomic ratio of 0.2%. The electrode with no Sb was inactive for EOP and showed very low stability. However, increasing the concentration of Sb results in a drastic change of the current efficiency that reaches ~48% at Sb/Sn atomic ratio of 2%. Higher concentrations of this element decrease the amount of produced ozone. The effect of Ni at a fixed concentration of Sb (Sb : Sn atomic ratio of 2 : 100) on Φ_{EOP} is shown in Figure 6(b). It is clear that Φ_{EOP} for the electrode without Ni is very small. However, the presence of a small amount of Ni (Ni : Sn atomic ratio of 0.2 : 100) has a profound effect on its ozone production capability and increases Φ_{EOP} to more

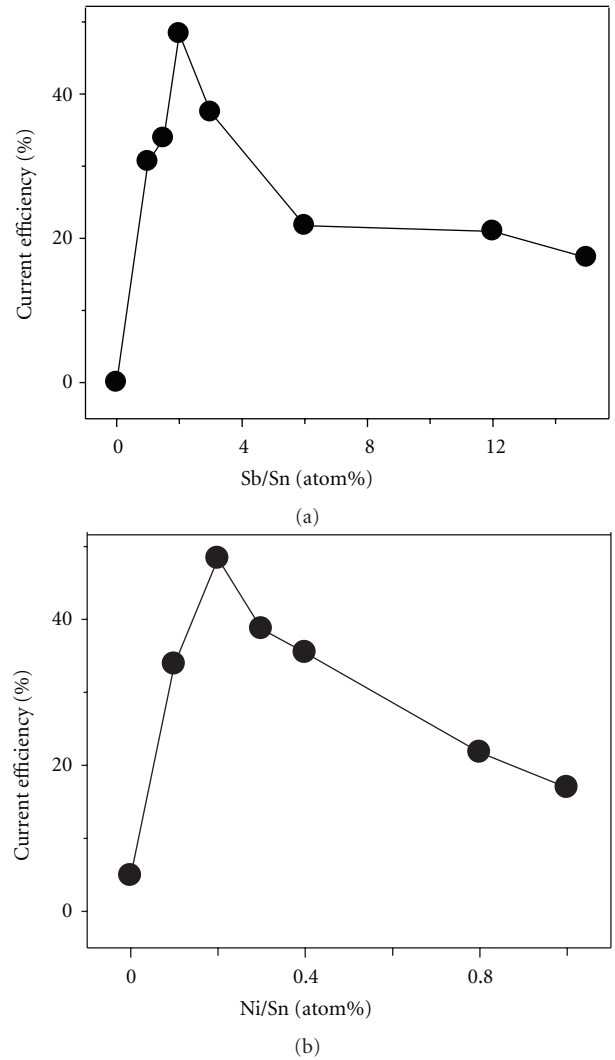

FIGURE 6: The effect of (a) Sb concentration in Ti/SnO_2-Sb(x%)-Ni(0.2%) and (b) Ni concentration in Ti/SnO_2-Sb(2%)-Ni(x%) electrodes on the current efficiency for EOP in 0.1 M H_2SO_4 at room temperature at an applied current density of 12 mA cm^{-2}. The values in parentheses are atomic ratios with respect to Sn.

than 48%. More Ni concentrations reduce Φ_{EOP} as shown in Figure 6(b). Therefore, the optimum composition of the electrode was Sn : Sb : Ni atomic ratio of 100 : 2 : 0.2, which provides a current efficiency of 48.3% for ozone generation in 0.1 M H_2SO_4 solution at room temperature. The optimum electrode composition obtained for EOP in the present work is comparable with those reported by Wang et al. (500 : 8 : 1) [30] and Christensen et al. (500 : 8 : 3) [22].

3.3. Kinetics of OER and EOP. In order to investigate the kinetics of the OER and EOP on the electrodes with different nickel and antimony contents, polarization curves were recorded under quasistationary conditions at potential sweep rate of 1 mV s^{-1} in 0.1 M H_2SO_4 solution. The Tafel plots were used to evaluate the kinetic parameters. To ensure that the hysteresis phenomena associated with the electrode response is absent and Tafel curves are reproducible, each

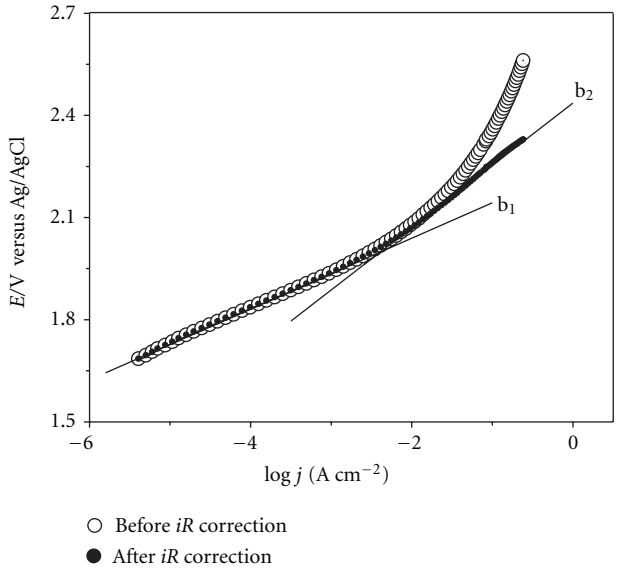

Figure 7: Typical Tafel curves for the Ti/SnO_2-Sb-Ni electrode with Sn : Sb : Ni of 100 : 2 : 0.2 before and after iR correction in 0.1 M H_2SO_4 solution at 25 ± 1°C. scan rate: 1 mV s^{-1}.

potential scan (both forward and backward) was recorded twice without interruption [19]. All empirical Tafel curves in the high overpotential region showed a deviation from linearity due to the ohmic drop effect. (4) shows the effect of ohmic drop (iR_Ω) on the polarization curve:

$$E = iR_\Omega + a + b \log i. \tag{4}$$

By taking $\log i = X$ and consequently $i = 10^X$, (4) can be transformed into (5)

$$E = 10^X R_\Omega + a + bX. \tag{5}$$

Equation (5) can be used to fit the experimental data by the least square method. The resulting values of a, b, and R_Ω would be acceptable providing that the correlation coefficient of fitting the data is ≥0.9999. This results in a single value for the Tafel slope (b) at low and high overpotential domains. A single value of b indicates that deviation from linearity is exclusively due to ohmic resistance and the electrode kinetics for the entire range remains unchanged. On the other hand, if the correlation coefficient for the entire data range of an electrode was <0.9999, the fitting would be considered unsatisfactory. In this case, the method is applied for the high overpotential region, where the influence of ohmic drop is more pronounced, and R_Ω as well as a value of b_2 can be successfully determined. Moreover, by applying the quantity of R_Ω in (4), the corresponding Tafel slope (b_1) can be determined from the low overpotential data. The presence of two linear segments in the Tafel plots after iR_Ω correction demonstrates that deviation from linearity in the high current region, in addition to ohmic resistance, is due to the change in kinetics, for example, rate determining step (rds) and/or apparent electronic transfer coefficient (α) [1, 10, 20]. A typical Tafel curve before and after iR_Ω correction is shown in Figure 7.

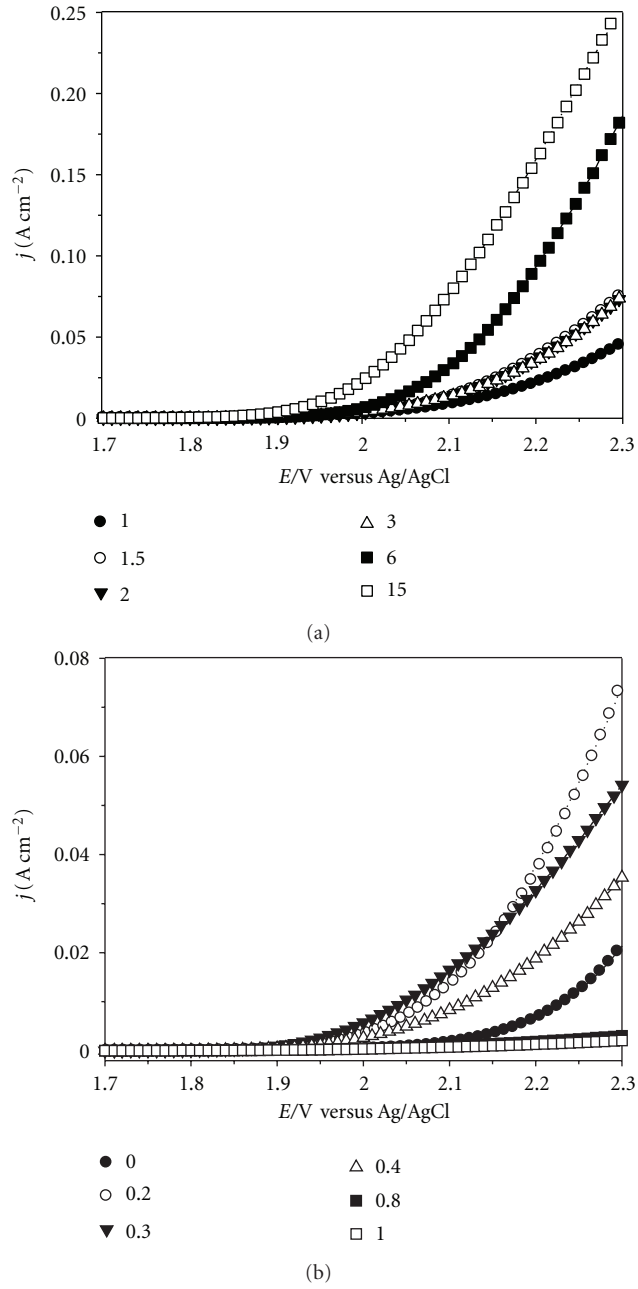

Figure 8: Linear sweep voltammograms of Ti/SnO_2-Sb(x%)-Ni(0.2%) electrodes at different Sb contents (a) and Ti/SnO_2-Sb(2%)-Ni(x%) electrodes at different Ni contents (b) in o.1 M H_2SO_4 solution at 25 ± 1°C. Scan rate: 1 mV S^{-1}. The values in parentheses are atomic ratios with respect to Sn.

3.3.1. The Effect of Sb Concentration on the Electrode Kinetics. The linear sweep voltammograms (LSVs) of the electrodes with different Sb contents are shown in Figure 8(a), indicating that the activity of the electrode toward solvent oxidation increases with increasing the concentration of this element. On the other hand, according to Figure 6(a), EOP decreases when Sb/Sn atomic ratio of the electrode exceeds 2%. Therefore, it can be concluded that OER is greatly enhanced over EOP on the electrodes with Sb/Sn >2 atom%. The empirical Tafel curves for the electrodes

with different Sb content were drawn from the voltammetric data of Figure 8(a) and, after *iR* correction, the Tafel slopes (b) and electronic transfer coefficients (α) at low and high overpotential domains were calculated (Table 1). As can be seen in Table 1, the resulting R_Ω-values (0.64–1.24 Ohm), which are the sum of R_{solution} and R_{film} for the electrodes with different Sb content, are in agreement with the R_Ω data obtained for other oxide electrodes in acidic electrolytes [19, 37–39].

Accepting the following reasonable mechanism of simultaneous OER/EOP processes on the inert electrodes proposed by Da Silva et al. [10], the empirical high Tafel slopes, b_1 and b_2, suggest that primary water discharge (6) is the rds on the present electrodes.

$$H_2O \longrightarrow (OH^\bullet)_{ads} + H^+ + e^- \quad (6)$$

$$(OH^\bullet)_{ads} \longrightarrow (O^\bullet)_{ads} + H^+ + e^- \quad (7)$$

$$2(O^\bullet)_{ads} \longrightarrow (O_2)_{ads} \longrightarrow O_2 \quad (8)$$

$$(O^\bullet)_{ads} + (O_2)_{ads} \longrightarrow (O_3)_{ads} \longrightarrow O_3 \quad (9)$$

According to the above mechanism, not all the O_2 formed leads to O_3. Indeed, O_3 formation is a chemical step (not electrochemical) and severely depends on the partial surface concentration of O_2 and $O^\bullet$ and of course an effective encounter between the oxygen intermediates, (9).

Considering primary water discharge as the rds and applying the kinetic treatment proposed by Bockris [40], the Tafel coefficient can be given by $b = 2.302RT/\alpha F$, where α is the apparent (effective) transfer coefficient for the non ideal case [10, 20]. All other parameters have their usual meaning. This equation leads to a theoretical Tafel slope of 120 mV at 25°C if it is assumed that α has its classical value of 0.5. It can be seen from Table 1, that changing the concentration of Sb in the electrode only changes the second Tafel slope (b_2) while the first one almost remained unchanged ($b_1 = 103.5 \pm 1$ mV). As suggested by Boodts and coworkers [10, 19], a different analysis can be performed using the apparent electronic transfer coefficient calculated from the experimental b-values, $\alpha = 2.302RT/bF$. It is possible to interpret the high b-values based on the assumption that changes take place in α. Indeed, according to classical electron transfer theory [41], α is an intrinsic parameter of the charge-transfer reaction at a particular interface. Therefore, considering that changes in α-value reflect modifications in the energy barrier for the electron transfer, these values can be used to correlate the influence of the chemical nature of the electrode with the energy barrier of the electron transfer process.

Table 1 presents the values of α, at low (OER), α_1, and high (OER/EOP), α_2, overpotentials, calculated for the electrodes with different Sb contents. In the low overpotential domain (Column 3, entries 1–6), the Sb content has no significant influence on α_1. The α_1-values around 0.57 were obtained for all the electrodes with varying Sb content. However, in the case of the high overpotential domain (Column 5, entries 1–6) a significant dependence of α_2 on the concentration of Sb is observed, that is, as the Sb content increases, the energy barrier for the electron transfer process decreases and the solvent oxidation facilitates. Highest α-value is presented by the electrodes containing Sb/Sn atomic ratio of more than 2%, which seems to affect the kinetics by decreasing the activation barrier for the OER process. However, according to Figure 6(a), EOP decreases when Sb/Sn atomic ratio of the electrode exceeds 2%. Therefore, it can be concluded that OER is greatly enhanced over EOP on the electrodes with Sb/Sn >2 atom%.

Table 1: Tafel slopes (b) and electronic transfer coefficients (α) at low (subscript 1) and high (subscript 2) overpotential domains, and ohmic resistance of Ti/SnO_2-Sb-Ni electrodes prepared with different Sb and Ni atom%.

Electrode*	b_1	α_1	b_2	α_2	R_Ω (Ohm)
Ti/SnO_2-Sb(1)-Ni(0.2)	104.5	0.57	202.5	0.27	1.24
Ti/SnO_2-Sb(1.5)-Ni(0.2)	102.5	0.58	183.2	0.32	0.97
Ti/SnO_2-Sb(2)-Ni(0.2)	103.2	0.57	176.5	0.34	1.01
Ti/SnO_2-Sb(3)-Ni(0.2)	102.7	0.58	173.8	0.34	1.02
Ti/SnO_2-Sb(6)-Ni(0.2)	102.7	0.58	131.9	0.45	0.64
Ti/SnO_2-Sb(15)-Ni(0.2)	103.8	0.57	122.2	0.48	0.74
Ti/SnO_2-Sb(2)-Ni(0)	155.6	0.38	155.6	0.38	0.96
Ti/SnO_2-Sb(2)-Ni(0.2)	103.2	0.57	176.5	0.34	1.01
Ti/SnO_2-Sb(2)-Ni(0.3)	107.4	0.55	170.1	0.35	2.77
Ti/SnO_2-Sb(2)-Ni(0.4)	110.1	0.54	179.6	0.33	3.30
Ti/SnO_2-Sb(2)-Ni(0.8)	183.3	0.32	310.5	0.19	27.61
Ti/SnO_2-Sb(2)-Ni(1)	184.2	0.32	333.0	0.18	37.11

* The values in parentheses are mole ratios in % with respect to Sn.

3.3.2. The Effect of Ni Concentration on Electrode Kinetics. Figure 8(b) presents the LSVs of the electrodes with different Ni contents. It is clear from this figure that only small amounts of Ni (Ni/Sn = 0.2 atom%) in the film increase the electrode activity toward solvent oxidation, which is in favor of EOP as shown in Figure 6(b). Higher Ni concentrations strongly reduce the activity of the electrodes. It should be pointed out that, although Ni doping in Ti/SnO_2-Sb electrode is necessary for EOP, its overdoping is pernicious to the electrode activity for solvent oxidation (for both EOP and OER). The empirical Tafel curves for the electrodes with different Ni content were drawn from the voltammetric data of Figure 8(b) and, after *iR* correction (as described in Section 3.3), the Tafel slopes and electronic transfer coefficients (α) at low and high overpotential domains were calculated (Table 1). The values of the ohmic resistance are also presented in Table 1. These values are the summation of R_{solution} and R_{film}. Since the distance of the working electrode and the capillary tip was the same in all experiments, the changes of the ohmic resistance of the electrodes with different Ni/Sn% can be attributed to the film resistance of these electrodes. In fact, introduction of Ni into the electrode structure increases their film resistance, which is more pronounced at higher Ni contents. These resistance variations are compatible to the results of Wang and

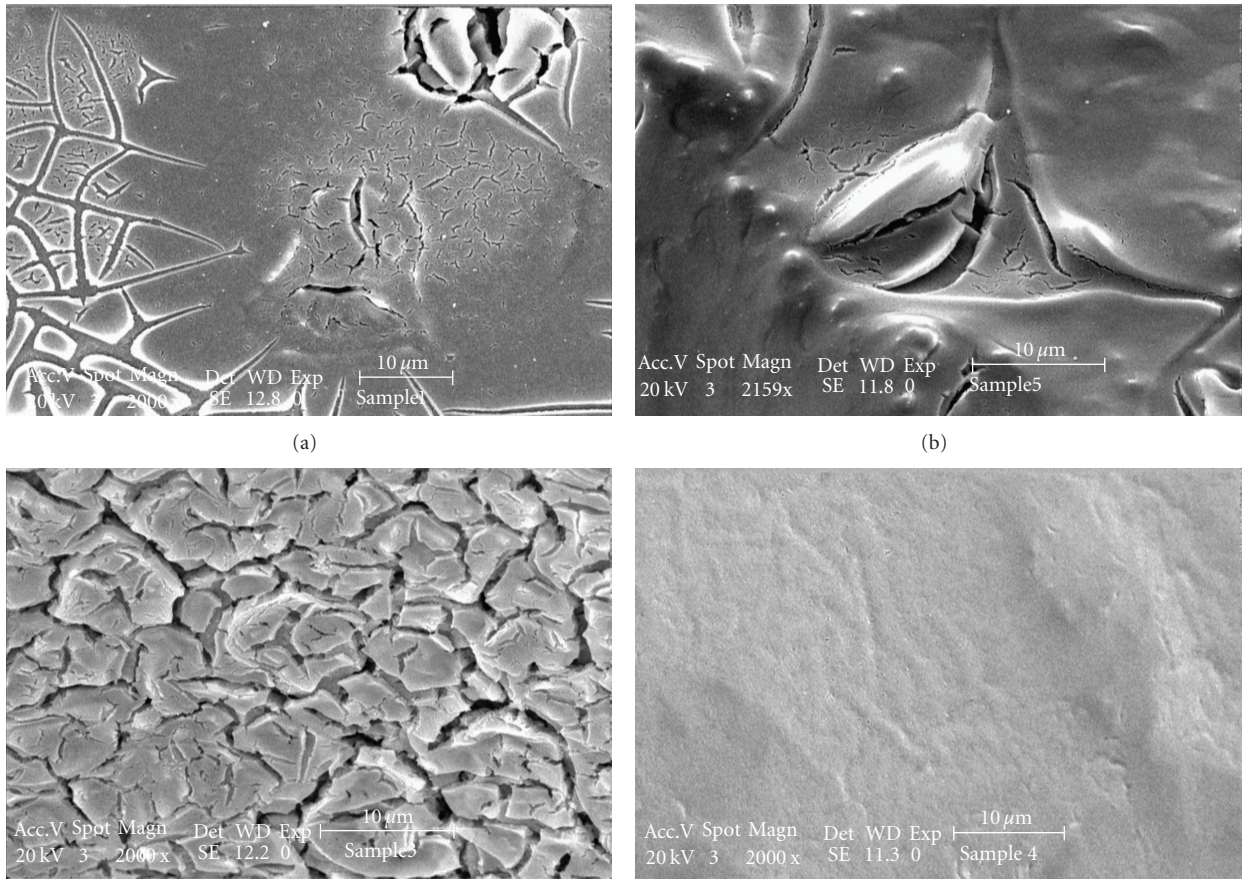

Figure 9: SEM images of freshly prepared (a) Ti/SnO_2-Sb(2%), (b) Ti/SnO_2-Sb(2%)-Ni(0.2%), (c) Ti/SnO_2-Sb(2%)-Ni(1%), and (d) Ti/SnO_2-Sb(12%)-Ni(0.2%) electrodes. The values in parentheses are atomic ratios with respect to Sn.

coworkers obtained by 4-probe resistivity meter [32] and describes lower capacitance of the electrodes with higher Ni content (Section 3.1).

Among the prepared electrodes, only the electrode with no Ni content presents a single Tafel slope in the low and high overpotential regions ($b_1 = b_2 = 155.6$, Table 1, entry 7), demonstrating that the primary water discharge is the rds and the kinetics of this electrode remains unchanged over the entire range of overpotentials ($\alpha_1 = \alpha_2 = 0.38$). However, the presence of Ni strongly affects the kinetics of the electrode. The Tafel curves for the electrodes containing small amounts of Ni (0.2–0.4%), after *iR* correction, show two distinct linear segments. Although b_1 and b_2 values reveal the primary water discharge as the rds, variation of b-values can be attributed to the changes in α. As can be seen in Table 1, the electrodes containing 0.2–0.4 atom% Ni have nearly the same values of α_1 (~0.56) and α_2 (~0.34), suggesting similarity of their kinetics at each of low and high overpotential regions, although the higher the Ni content the higher the resistance of the electrode. More addition of Ni into the electrode structure drastically increases the electrode resistance and diminishes both of the α_1 and α_2 values (Table 1, entries 11 and 12).

The above results indicate that high concentration of Ni in the electrode affects the kinetics by increasing the activation barrier of the electron transfer [42]. Moreover, these observations indicate that OER and EOP kinetics strongly depend on the presence of Ni and its concentration. This is in accordance with the increase in electrode film resistances (Table 1) and the decrease in EOP current efficiency (Figure 6) on these electrodes by increasing Ni concentration.

3.4. Surface Morphology and XRD Analysis. Figure 9 shows representative SEM images of the chemically modified titanium mesh electrodes. The surface morphology presents a dependence on both Ni and Sb content. In the case of the electrode with no Ni content (Sn : Sb atomic ratio of 100 : 2), Figure 9(a), one observes an inhomogeneous microstructure characterized by some flat and compact surface regions surrounded by cracked areas showing mud structure. This type of morphology is typical of oxide electrodes prepared by thermal decomposition [34, 43, 44]. The cracks were likely produced on the surface during the cooling of the electrode to room temperature.

The introduction of small amounts of Ni (Ni/Sn atomic ratio of 0.2%) into the electrode structure significantly affects the coating morphology. As shown in Figure 9(b), the surface of the Ti/SnO_2-Sb-Ni with Sn : Sb : Ni atomic ratio of 100 : 2 : 0.2 is more compact with less cracks. Addition of more Ni into the oxide layer results in mud structure coatings

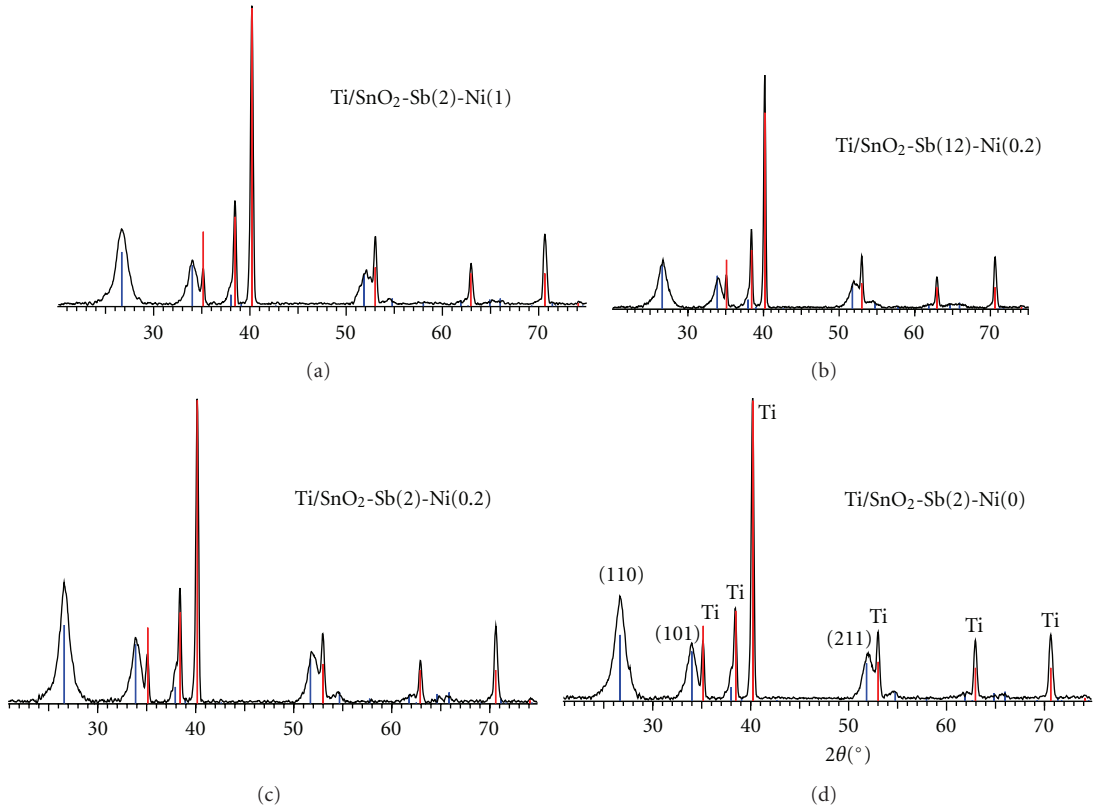

Figure 10: Typical XRD patterns of Ti/SnO_2-Sb-Ni electrodes with different amounts of antimony and nickel. The values in parentheses are atomic ratios in % with respect to Sn. The peaks marked with blue lines are related to SnO_2.

with deeper cracks. This is typically shown in Figure 9(c) for the surface of the electrode with Sn : Sb : Ni atomic ratio of 100 : 2 : 1. Increasing the Sb content while the concentration of Ni/Sn is fixed at 0.2 atom% results in homogeneous and fully compact structure as shown in Figure 9(d).

Figure 10 shows typical XRD patterns of SnO_2 on Ti foil containing different concentrations of Sb and Ni. In addition to the peaks corresponding to the Ti support, there are several peaks that agree well with the (1 1 0), (1 0 1), and (2 1 1) reflections of a rutile-type structure due to SnO_2 cassiterite. No characteristic peaks of other phases such as Sb or Ni oxides were detected, indicating that all Sb and Ni are in the ionic form that came into the crystal lattice of bulk SnO_2 to substitute for Sn ions. These observations are in agreement with the results of Kong et al. [43] and Montilla et al. [45] on Ti/SnO_2-Sb electrodes prepared by thermal decomposition method. Because the SnO_2 (1 1 0) diffraction peak is completely isolated from the Ti substrate peaks, it can be used to calculate the average crystallite size of the particles from FWHM of the diffraction peak according to Scherrer's equation. The unit-cell parameters of the electrodes were calculated using the Bragg's formula and assuming tetragonal SnO_2 crystals.

Table 2 presents the lattice parameters (a = b, and c), unit-cell volumes (V), and crystallite sizes obtained for different electrodes. It can be seen that insertion of Sb and Ni into the SnO_2 matrix resulted in significant changes in these parameters. Among different compositions investigated, the electrode with Sb/Sn and Ni/Sn atomic ratios of 2% and 0.2%, respectively, (Sn : Sb : Ni atomic ratio of 100 : 2 : 0.2) showed increase in the lattice parameters, unit-cell volume, and crystallite size (Table 2, entry 3) compared to standard SnO_2. The SnO_2 crystallite size of this electrode is also the largest among the electrodes studied. The values of these parameters decrease for other electrode compositions (Table 2, entries 2, 4, and 5). Wang et al. [32], from XPS data analysis, showed that all the Sb and Ni doped in SnO_2 electrodes have the valences of +5 and +3, respectively. Therefore, with the exception of the electrode with Sn : Sb : Ni atomic ratio of 100 : 2 : 0.2, the lower lattice parameters and the unit-cell volume for the electrodes presented in Table 2, can be explained due to the formation of solid solutions between SnO_2, Sb, and Ni by substitution of Sn^{4+} ions (ionic radius of 0.83 Å) in the cassiterite structure by Sb^{5+} and Ni^{3+} ions which have lower ionic radii of 0.74 and 0.72 Å, respectively. These observations are in agreement with those of Montilla et al. on Ti/SnO_2-Sb electrodes [45]. However, the reason for increase of lattice parameters, unit-cell volume, and crystallite size of the electrode with Sn : Sb : Ni atomic ratio of 100 : 2 : 0.2 is not clear to us, but it may describe the unique electrochemical behavior of this electrode and its high ozone production efficiency (see Section 3.2).

3.5. Investigation of Electrode Stability. Many efforts have been done to improve the service life of Sb-doped SnO_2 electrodes under the anodic polarization conditions in acidic

Table 2: Lattice parameters (a = b, and c), unit cell volume (V), and crystallite size of four different Ni-and Sb-doped SnO_2 films coated on Ti substrate.

Electrode[a]	Lattice parameters/Å		Unit cell volume/Å^3	SnO_2 crystallite size (nm)
	a	c		
SnO_2 cassiterite[b]	4.738	3.187	71.54	—
Ti/SnO_2-Sb(2)-Ni(0)	4.738	3.181	71.40	7.0
Ti/SnO_2-Sb(2)-Ni(0.2)	4.742	3.189	71.71	7.4
Ti/SnO_2-Sb(2)-Ni(1)	4.736	3.176	71.24	6.6
Ti/SnO_2-Sb(12)-Ni(0.2)	4.722	3.175	70.81	6.1

[a]The values in parentheses are mole ratios in % with respect to Sn.
[b]According to the instrument library.

media [33, 44, 46]. The effect of composition on the stability of the electrodes was investigated by performing accelerated life tests under anodic polarization of 200 mA cm^{-2}. The anode potential was recorded as a function of time. The service life of the electrode is defined here as the operation time at which the anodic potential increases rapidly by 5 V versus the reference electrode, under galvanostatic conditions (i = 200 mA cm^{-2}) in 0.1 M H_2SO_4 solution.

Figure 11(a) shows the stability of the electrode as a function of Sb doping ratio, indicating that the service life of the electrode increases with increasing the Sb doping level up to Sb/Sn atom ratio of 12%. This is in good agreement with the SEM results on this electrode which indicate compactness of the electrode containing relatively high Sb concentration, Figure 9(d). Nevertheless, as discussed in Section 3.2, the Sb/Sn atomic ratio of more than 2% reduces the EOP current efficiency in favor of OER. Variation of the service life of the electrode containing 2 atom% of Sb as a function of Ni content is shown in Figure 11(b). It is evident that small amounts of Ni (Ni/Sn of 0.2 atom%) sharply increases the service life and EOP current efficiency of the electrode. Higher Ni concentrations drastically reduce the service life of the electrode. Rapid destruction of the electrodes with relatively high Ni content (Ni/Sn >0.2 atom%) can be mainly related to their high film resistance (see Section 3.3.2 and Table 1 entries 7–12). It is interesting to note that the service life and current efficiency of the electrode for EOP (see Figure 6) both follow the same trend, that is, introduction of a small amount of Ni (Ni/Sn of 0.2 atom%) into the electrode structure increases both its stability and EOP efficiency.

Figures 12(a) and 12(b) show the SEM microstructures of the Ti/SnO_2-Sb electrode with Sb/Sn of 2 atom% after the service life test. It can be seen that the surface texture of the electrode has been destroyed and there are many fractures and holes on the film surface as compared to the corresponding freshly prepared electrode shown in Figure 9(a). The edges of these fractures are oriented outside of the electrode surface, which can be related to erosion provoked by the intense gas bubble formation from inside of the layer produced during the anodic polarization of the electrode. This results finally in detachment of the catalyst layer from the electrode surface. Figure 12(c) shows the SEM micrograph of the Ti/SnO_2-Sb-Ni (Sn : Sb : Ni atomic ratio

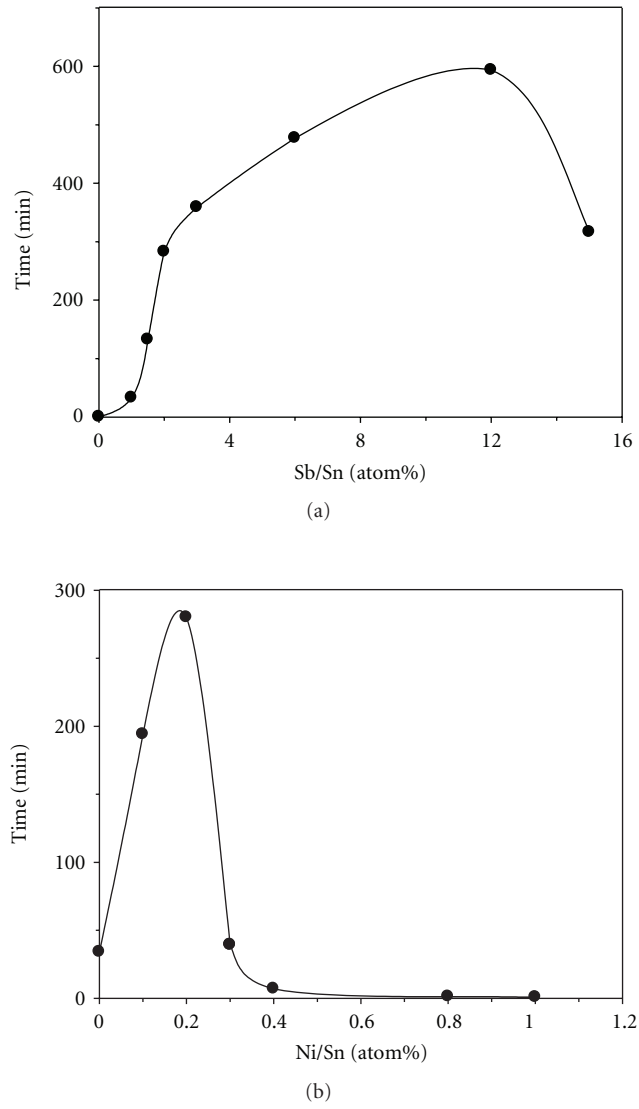

Figure 11: Dependence of service life times of (a) Ti/SnO_2-Sb(x%)-Ni(0.2%) electrodes on Sb% and (b) Ti/SnO_2-Sb(2%)-Ni(x%) electrodes on Ni%. The life times were obtained by the accelerated life tests under current density of 200 mA cm^{-2} in 0.1 M H_2SO_4 solution. The values in parentheses are atomic ratios with respect to Sn.

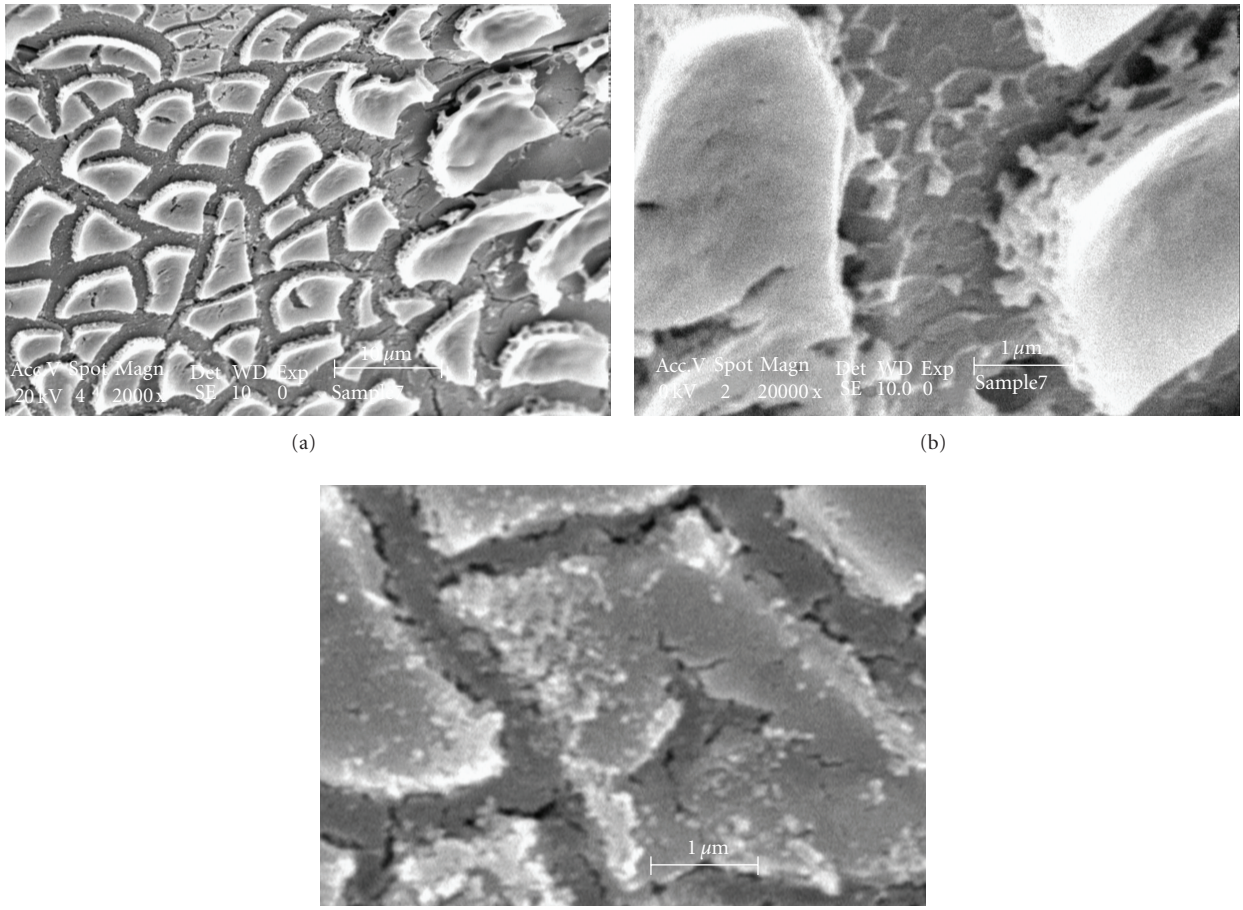

Figure 12: SEM images of (a) and (b) deactivate Ti/SnO_2-Sb (Sb : Sn of 100 : 2) electrode at different magnifications and (c) deactivated Ti/SnO_2-Sb-Ni (Sn : Sb : Ni of 100 : 2 : 0.2) electrode.

of 100 : 2 : 0.2) electrode after service life test. Comparing this image with the corresponding freshly prepared electrode, Figure 9(b), indicates that a large number of cracks have been formed on the surface during the anodic polarization, presumably due to erosion. Nevertheless, comparing the deactivated Ti/SnO_2-Sb (Sb : Sn atomic ratio of 100 : 2) and Ti/SnO_2-Sb-Ni (Sn : Sb : Ni atomic ratio of 100 : 2 : 0.2) electrodes (Figures 12(b) and 12(c), resp.) indicates much more stability of the latter electrode. In fact, introducing a small amount of Ni into the electrode increases its surface compactness and improves its resistance against destruction during the intense anodic polarization.

4. Conclusions

Ti/SnO_2-Sb-Ni electrodes with various Ni and Sb dopant levels were prepared by dip-coating thermal pyrolysis technique. The prepared electrodes have a rutile-type structure due to SnO_2 cassiterite without any other phases such as Sb or Ni oxides. In fact, all Sb and Ni contents are present in ionic form substituted for Sn ions in the crystal lattice of bulk SnO_2. The surface morphology of the electrodes strongly depends on both Ni and Sb contents.

The surface compactness of the Ti/SnO_2-Sb-Ni electrodes as well as their capacitance, roughness factor, and service life depend on Sb doping level and increase with increasing the concentration of this element up to an Sb/Sn atomic ratio of 12%. Empirical Tafel slopes obtained for both low and high overpotential regions indicate the primary water discharge as the rds. The values of Tafel slopes were attributed to the apparent electronic transfer coefficient (α). Increasing the Sb content has no significant effect on α_1 but significantly enhances the α_2 values. In fact in the high overpotential domain, increasing the Sb content diminishes the energy barrier of the electron transfer process and facilitates the electron transfer for solvent oxidation. However, EOP decreases when Sb/Sn ratio of the electrode exceeds 2 atom%. In fact, OER is greatly enhanced over EOP on the electrodes with Sb/Sn >2 atom%.

The structure and properties of the Ti/SnO_2-Sb-Ni electrodes strongly depend on the Ni concentration. The current efficiency for ozone production on Ti/SnO_2-Sb electrodes is very low and OER is predominant. Addition of a small amount of Ni into the electrode structure has a profound effect on its EOP capability. The capacitance and roughness factor of the electrodes decrease whereas their film

resistance increase with increasing Ni concentration. All the empirical Tafel slopes (b_1 and b_2) of the electrodes containing different Ni concentrations point to the primary water discharge as the rds. Here again the Tafel slopes were related to the apparent electronic transfer coefficient (α). While Ti/SnO_2-Sb electrode has a single Tafel slope at low and high overpotential regions, the presence of a small amount of Ni changed the electrode kinetics at both overpotential regions and two different α values were obtained. It should be pointed out that only a small amount of Ni increases the service life as well as the activity of the electrode in favor of EOP. Increasing of Ni/Sn atomic ratio beyond 0.2% results in very low capacitance and roughness factor. Moreover, high doping level of Ni increases the film resistance, decreases the service life of the electrodes, and lowers their EOP efficiency.

Highest current efficiency (48.3%) for EOP was achieved on the electrode containing Sb/Sn and Ni/Sn atomic ratios of 2% and 0.2%, respectively, at a current density of $12\,mA\,cm^{-2}$ in 0.1 M H_2SO_4 solution. Although Ti/SnO_2-Sb-Ni electrode is efficient for EOP, still more investigations are needed to improve its durability and EOP efficiency, and to better understand the mechanism of simultaneous EOP and OER.

Acknowledgments

This work was financially supported by the Research Council and Center of Excellence for Catalyst and Fuel Cell of the University of Isfahan and Iranian Nanotechnology Initiative Council.

References

[1] L. M. Da Silva, L. A. De Faria, and J. F. C. Boodts, "Green processes for environmental application. Electrochemical ozone production," *Pure and Applied Chemistry*, vol. 73, no. 12, pp. 1871–1884, 2001.

[2] C. Gottschalk, J. A. Libra, and A. Saupe, *Ozonation of Water and Waste Water*, Wiley-VCH, Weinheim, Germany, 2002.

[3] K. Ikehata and M. G. El-Din, "Aqueous pesticide degradation by ozonation and ozone-based advanced oxidation processes: a review (part I)," *Ozone: Science and Engineering*, vol. 27, no. 2, pp. 83–114, 2005.

[4] D. V. Franco, W. F. Jardim, J. F. C. Boodts, and L. M. Da Silva, "Electrochemical ozone production as an environmentally friendly technology for water treatment," *Clean*, vol. 36, no. 1, pp. 34–44, 2008.

[5] R. Neumann and A. M. Khenkin, "Alkane oxidation with manganese substituted polyoxometalates in aqueous media with ozone and the intermediacy of manganese ozonide species," *Chemical Communications*, no. 18, pp. 1967–1968, 1998.

[6] L. M. Da Silva, M. H. P. Santana, and J. F. C. Boodts, "Electrochemistry and green chemical processes: Electrochemical ozone production," *Quimica Nova*, vol. 26, no. 6, pp. 880–888, 2003.

[7] P. C. Foller and C. W. Tobias, "Anodic evolution of ozone," *Journal of the Electrochemical Society*, vol. 129, no. 3, pp. 506–515, 1982.

[8] P. Tatapudi and J. M. Fenton, "Simultaneous synthesis of ozone and hydrogen peroxide in a proton-exchange-membrane electrochemical reactor," *Journal of the Electrochemical Society*, vol. 141, no. 5, pp. 1174–1178, 1994.

[9] R. Amadelli, L. Armelao, A. B. Velichenko et al., "Oxygen and ozone evolution at fluoride modified lead dioxide electrodes," *Electrochimica Acta*, vol. 45, no. 4-5, pp. 713–720, 1999.

[10] L. M. Da Silva, L. A. De Faria, and J. F. C. Boodts, "Electrochemical ozone production: Influence of the supporting electrolyte on kinetics and current efficiency," *Electrochimica Acta*, vol. 48, no. 6, pp. 699–700, 2003.

[11] K. Onda, T. Ohba, H. Kusunoki, S. Takezawa, D. Sunakawa, and T. Araki, "Improving characteristics of ozone water production with multilayer electrodes and operating conditions in a polymer electrolyte water electrolysis cell," *Journal of the Electrochemical Society*, vol. 152, no. 10, pp. D177–D183, 2005.

[12] A. A. Babak, R. Amadelli, and V. N. Fateev, "Effect of perfluoro compounds on kinetics of the oxygen and ozone formation at the platinum anode," *Russian Journal of Electrochemistry*, vol. 34, no. 2, pp. 149–152, 1998.

[13] M. I. Awad, M. M. Saleh, and T. Ohsaka, "Ozone electrogeneration on Pt-loaded reticulated vitreous carbon using flooded and flow-through assembly," *Journal of the Electrochemical Society*, vol. 153, no. 12, Article ID 055612JES, pp. D207–D212, 2006.

[14] M. I. Awad, S. Sata, K. Kaneda, M. Ikematsu, T. Okajima, and T. Ohsaka, "Ozone electrogeneration at a high current efficiency using a tantalum oxide-platinum composite electrode," *Electrochemistry Communications*, vol. 8, no. 8, pp. 1263–1269, 2006.

[15] K. Kaneda, M. Ikematsu, Y. Koizumi et al., "Ozone generation by a TaO_x and Pt composite insulator-coated Ti electrode," *Electrochemical and Solid-State Letters*, vol. 8, no. 6, pp. J13–J16, 2005.

[16] S.-G. Park, G.-S. Kim, J.-E. Park, Y. Einaga, and A. Fujishima, "Use of boron-doped diamond electrode in ozone generation," *Journal of New Materials for Electrochemical Systems*, vol. 8, no. 1, pp. 65–68, 2005.

[17] K. Arihara, C. Terashima, and A. Fujishima, "Electrochemical production of high-concentration ozone-water using freestanding perforated diamond electrodes," *Journal of the Electrochemical Society*, vol. 154, no. 4, pp. E71–E75, 2007.

[18] A. Kraft, M. Stadelmann, M. Wünsche, and M. Blaschke, "Electrochemical ozone production using diamond anodes and a solid polymer electrolyte," *Electrochemistry Communications*, vol. 8, no. 5, pp. 883–886, 2006.

[19] L. M. Da Silva, D. V. Franco, L. A. De Faria, and J. F. C. Boodts, "Surface, kinetics and electrocatalytic properties of Ti/(IrO_2 + Ta_2O_5) electrodes, prepared using controlled cooling rate, for ozone production," *Electrochimica Acta*, vol. 49, no. 22-23, pp. 3977–3988, 2004.

[20] M. H. P. Santana, L. A. De Faria, and J. F. C. Boodts, "Investigation of the properties of Ti/[IrO_2-Nb_2O_5] electrodes for simultaneous oxygen evolution and electrochemical ozone production, EOP," *Electrochimica Acta*, vol. 49, no. 12, pp. 1925–1935, 2004.

[21] K. Kitsuka, K. Kaneda, M. Ikematsu, M. Iseki, K. Mushiake, and T. Ohsaka, "N-type TiO_2 thin films for electrochemical ozone production," *Journal of the Electrochemical Society*, vol. 157, no. 2, pp. F30–F34, 2010.

[22] P. A. Christensen, W. F. Lin, H. Christensen et al., "Room temperature, electrochemical generation of ozone with 50% current efficiency in 0.5 M sulfuric acid at cell voltages <3 V," *Ozone: Science and Engineering*, vol. 31, no. 4, pp. 287–293, 2009.

[23] Y. H. Wang, S. Cheng, and K. Y. Chan, "Synthesis of ozone from air via a polymer-electrolyte-membrane cell with a doped tin oxide anode," *Green Chemistry*, vol. 8, no. 6, pp. 568–572, 2006.

[24] C. Goebbert, R. Nonninger, M. A. Aegerter, and H. Schmidt, "Wet chemical deposition of ATO and ITO coatings using crystalline nanoparticles redispersable in solutions," *Thin Solid Films*, vol. 351, no. 1-2, pp. 79–84, 1999.

[25] J. Zhang and L. Gao, "Synthesis of antimony-doped tin oxide (ATO) nanoparticles by the nitrate-citrate combustion method," *Materials Research Bulletin*, vol. 39, no. 14-15, pp. 2249–2255, 2004.

[26] X. Chen, F. Gao, and G. Chen, "Comparison of Ti/BDD and Ti/SnO_2-Sb_2O_5 electrodes for pollutant oxidation," *Journal of Applied Electrochemistry*, vol. 35, no. 2, pp. 185–191, 2005.

[27] F. Montilla, E. Morallón, and J. L. Vázquez, "Evaluation of the electrocatalytic activity of antimony-doped tin dioxide anodes toward the oxidation of phenol in aqueous solutions," *Journal of the Electrochemical Society*, vol. 152, no. 10, pp. B421–B427, 2005.

[28] X. Y. Li, Y. H. Cui, Y. J. Feng, Z. M. Xie, and J. D. Gu, "Reaction pathways and mechanisms of the electrochemical degradation of phenol on different electrodes," *Water Research*, vol. 39, no. 10, pp. 1972–1981, 2005.

[29] C. L. P. S. Zanta, P. A. Michaud, C. Comninellis, A. R. De Andrade, and J. F. C. Boodts, "Electrochemical oxidation of p-chlorophenol on SnO_2-Sb_2O_5 based anodes for wastewater treatment," *Journal of Applied Electrochemistry*, vol. 33, no. 12, pp. 1211–1215, 2003.

[30] Y.-H. Wang, S. Cheng, K.-Y. Chan, and X. Y. Li, "Electrolytic generation of ozone on antimony- And nickel-doped tin oxide electrode," *Journal of the Electrochemical Society*, vol. 152, no. 11, pp. D197–D200, 2005.

[31] Y. Cui, Y. Wang, B. Wang, H. Zhou, K.-Y. Chan, and X.-Y. Li, "Electrochemical generation of ozone in a membrane electrode assembly cell with convective flow," *Journal of the Electrochemical Society*, vol. 156, no. 4, pp. E75–E80, 2009.

[32] Y. H. Wang, K. Y. Chan, X. Y. Li, and S. K. So, "Electrochemical degradation of 4-chlorophenol at nickel-antimony doped tin oxide electrode," *Chemosphere*, vol. 65, no. 7, pp. 1087–1093, 2006.

[33] G. Chen, X. Chen, and P. L. Yue, "Electrochemical behavior of novel Ti/IrO_x-Sb_2O_5-SnO_2 anodes," *Journal of Physical Chemistry B*, vol. 106, no. 17, pp. 4364–4369, 2002.

[34] F. Montilla, E. Morallón, A. De Battisti, and J. L. Vázquez, "Preparation and characterization of antimony-doped Tin dioxide electrodes. Part 1. Electrochemical characterization," *Journal of Physical Chemistry B*, vol. 108, no. 16, pp. 5036–5043, 2004.

[35] A. W. Bott, "Electrochemistry of semiconductors," *Current Separations*, vol. 17, no. 3, pp. 87–91, 1998.

[36] N. L. Wu, J. Y. Hwang, P. Y. Liu et al., "Synthesis and characterization of Sb-doped SnO_2 xerogel electrochemical capacitor," *Journal of the Electrochemical Society*, vol. 148, no. 6, pp. A550–A553, 2001.

[37] T. A. F. Lassali, J. F. C. Boodts, and L. O. S. Bulhões, "Faradaic impedance investigation of the deactivation mechanism of Ir-based ceramic oxides containing TiO_2 and SnO_2," *Journal of Applied Electrochemistry*, vol. 30, no. 5, pp. 625–634, 2000.

[38] L. A. Da Silva, V. A. Alves, M. A. P. Da Silva, S. Trasatti, and J. F. C. Boodts, "Oxygen evolution in acid solution on IrO_2 + TiO_2 ceramic films. A study by impedance, voltammetry and SEM," *Electrochimica Acta*, vol. 42, no. 2, pp. 271–281, 1997.

[39] J. M. Hu, H. M. Meng, J. Q. Zhang, and C. N. Cao, "Degradation mechanism of long service life Ti/IrO_2-Ta_2O_5 oxide anodes in sulphuric acid," *Corrosion Science*, vol. 44, no. 8, pp. 1655–1668, 2002.

[40] J. O. M. Bockris, "Kinetics of activation controlled consecutive electrochemical reactions: Anodic evolution of oxygen," *The Journal of Chemical Physics*, vol. 24, no. 4, pp. 817–827, 1956.

[41] J. O. M. Bockris and A. K. N. Reddy, *Modern Electrochemistry*, Plenum Press, New York, NY, USA, 1977.

[42] M. H. P. Santana, L. A. De Faria, and J. F. C. Boodts, "Effect of preparation procedure of IrO_2-Nb_2O_5 anodes on surface and electrocatalytic properties," *Journal of Applied Electrochemistry*, vol. 35, no. 9, pp. 915–924, 2005.

[43] J.-T. Kong, S.-Y. Shi, X.-P. Zhu, and J.-R. Ni, "Effect of Sb dopant amount on the structure and electrocatalytic capability of Ti/Sb-SnO_2 electrodes in the oxidation of 4-chlorophenol," *Journal of Environmental Sciences*, vol. 19, no. 11, pp. 1380–1386, 2007.

[44] B. Adams, M. Tian, and A. Chen, "Design and electrochemical study of SnO_2-based mixed oxide electrodes," *Electrochimica Acta*, vol. 54, no. 5, pp. 1491–1498, 2009.

[45] F. Montilla, E. Morallón, A. De Battisti, A. Benedetti, H. Yamashita, and J. L. Vázquez, "Preparation and characterization of antimony-doped Tin dioxide electrodes. Part 2. XRD and EXAFS characterization," *Journal of Physical Chemistry B*, vol. 108, no. 16, pp. 5044–5050, 2004.

[46] F. Montilla, E. Morallón, A. De Battisti, S. Barison, S. Daolio, and J. L. Vázquez, "Preparation and characterization of antimony-doped tin dioxide electrodes. 3. XPS and SIMS characterization," *Journal of Physical Chemistry B*, vol. 108, no. 41, pp. 15976–15981, 2004.